

Summer monsoon rainfall trends in the Indian Himalayan region

Sandipan Mukherjee · Rajesh Joshi · Ram C. Prasad ·
Subhash C.R. Vishvakarma · Kireet Kumar

Received: 13 March 2014 / Accepted: 30 August 2014 / Published online: 16 September 2014
© Springer-Verlag Wien 2014

Abstract Impacts of the changing climatic regime on the trends of Indian summer monsoon rainfall (ISMR) are explored in this study for the Indian Himalayan region (IHR). The analysis is carried out for the period of 1951–2007 using a daily high resolution gridded data from APHRODITE project. At first, the percent departures of decadal rainfall are estimated from the long-term June to September rainfall values for the western, central, and eastern Himalayan (WH, CH, and EH) regions. Next, changes in the frequency of *strong* and *weak* phases of monsoon intra-seasonal oscillation are investigated. A non-parametric statistical method (Sen's slope estimator) is applied to the seasonal (i) mean rainfall, (ii) maximum rainfall, and (iii) frequency of extreme rainfall events of WH, CH, and EH regions to identify changes in their decadal, multiple year normals (NY1; 1951–1980 and NY2; 1981–2007) and long-term (NY3; 1951–2007) trends. The inter annual to inter decadal variabilities of the frequency of extreme rainfall events are explored by analyzing statistically significant intrinsic mode functions of the empirical mode decomposition (EMD) method. Results of our analyses have revealed existence of an alternative decadal oscillation of scanty and excessive summer monsoon rainfall trends for the WH, whereas excessive rainfall is observed in the last three decades (1980–2007) over the CH region. It is also observed that the frequencies of both monsoon *strong* and *weak* phases are decreasing for the entire Himalayan region. No significant trend is observed for the WH and CH regions for the normal periods NY1, NY2, and NY3 when

seasonal average rainfall is considered. However, a significant (p value < 0.05) negative trend of -0.04 mm/day rain is observed for the EH region during NY1 period. Similarly, the seasonal maximum rainfall trends for all the normal periods are found to be negative of which trends of -0.12 and -0.43 mm/day during NY3 and NY1 are observed for WH and EH regions, respectively (p value < 0.05). No significant enhancement in the extreme rainfall event frequencies is observed for the entire IHR during 1951–2007. However, a statistically insignificant positive trend in the extreme event frequencies is observed for the EH region. A dominant cycle of ~ 2.7 years of high frequency of extreme rainfall events is observed for all the regions whereas, a 12.2-, 15.3-, and 5.8-year cycles are observed for the WH, CH, and EH regions, respectively.

1 Introduction

It is now well accepted that the atmospheric surface layer temperature of the Earth is systematically increasing with a rate of 0.07 °C per decade due to change in climatic regimes (Jones and Moberg 2003). The rate enhancement of temperature has increased to 0.13 °C per decade in the last 50 years (IPCC 2007). Such an increasing trend of temperature has presumably affected the rainfall distribution across the world, particularly the Indian summer monsoon rainfall (ISMR), by modulating the moisture content of the atmosphere (Singh and Kumar 1997; Goswami et al. 2006; Rajeevan et al. 2006, 2008; Singh et al. 2008; Pattanaik and Rajeevan 2010).

The annual as well as summer monsoon rainfall over the Himalayan region is also assumed to be affected by climate change. Consequently, long-term rainfall distribution pattern for the Himalayan region has also been investigated

S. Mukherjee (✉) · R. Joshi · R. C. Prasad ·
S. C. R. Vishvakarma · K. Kumar
G.B. Pant Institute of Himalayan Environment and Development,
Kosi-Katarmal, Almora 263 643, Uttarakhand, India
e-mail: sandipanmukherjee@hotmail.com

by various researchers (Pant and Borgaonkar 1984; Pant et al. 1999; Shrestha et al. 2000; Sharma et al. 2000; Singh and Sen-Roy 2002; Fowler and Archer 2006; Kumar et al. 2005). Amongst these studies, few have reported positive trends (increasing seasonal and/ annual mean of rainfall) in the rainfall pattern for some local region such as Sharma et al. (2000) for Kosi basin in Nepal and Kumar et al. (2005) for the state of Himachal Pradesh in India; whereas negative rainfall trends are reported by others, for example Singh and Sen-Roy (2002) for Beas basin and Kumar and Jain (2010) for Qazigund and Kukarnag of Kashmir. Few reports have also concluded no significant trend of rainfall at all, such as Archer and Fowler (2004) for upper Indus basin; Khan (2001) for Jhelum river area of Pakistan, and Joshi et al. (2013) for Almora and Nainital stations of central Himalayan region in India. Such ambiguity in the trend of monsoon rainfall events, particularly for the extreme events, was also observed by Goswami et al. (2006) for the relatively homogeneous terrains of central India. Therefore, Goswami et al. (2006) have argued that the data and methodologies used for rainfall analyses are mostly responsible for this indiscernible trends of monsoon rainfall. Furthermore, Goswami et al. (2006) have also argued that short-duration extreme rain events are a consequence of small-scale convective instabilities in a moist atmosphere. This argument was further explored by Pattanaik and Rajeevan (2010) who have found that the increasing trend of extreme rainfall over central India is mainly contributed by synoptic scale systems having periodicity between 3 and 7 days.

However, the process of resolving the monsoon rainfall distribution pattern over complex terrains of the Himalaya is more difficult than the central India due to severe modification of precipitation processes by terrain induced wave such as the lee-wave and seeder-feeder mechanisms (Barry 2008). The orographic modulation of precipitation which is occurring due to synoptic scale uplift or convective instability is unrestrained. Hence, depending on the location and height of the mountain and nature of the convection, altitudinal and slope-wise (such as, south facing slope receives higher rainfall) variation of rainfall can be observed (Shrestha et al. 2000; Barros et al. 2004; Barry 2008). Therefore, identification of rainfall trend for a localized area or a station in a complex terrain may not necessarily represent the actual trend of the ISMR for the entire region as ISMR is a regional scale phenomena. As a consequence, a relatively large spatial domain is needed to identify changes in the rainfall trend. Therefore, in this study, trend of the ISMR over a relatively large spatial domain of the Indian Himalayan region (IHR) is explored with a comparatively high resolution observed-interpolated hybrid data addressing three different objectives. The first objective is to identify changes in the frequency of *strong* and *weak* phases of the 10–90 days low frequency intra-seasonal

oscillation of the ISMR over the IHR. The second objective of this study is to identify trends in the seasonal average and maximum rainfall for the IHR. The third objective is to identify cycles in the extreme rainfall event frequencies over the IHR using a nonlinear and non-stationary data analysis method. Investigation of the *strong* and *weak* phases of the monsoon-intra seasonal oscillation is of special importance as the duration and frequency of the *strong* and *weak* spells of ISMR have great influence on agriculture yields, disaster, and water resource management of the Indian sub-continent (Gadgil and Rao 2000). However, it is to be noted that the rainfall distribution over the entire Himalaya region is analyzed by segregating grids for the western, central, and eastern regions and no attempt is made to distinguish rainfall distribution for the IHR and Himalayan foothills. Again, it is to be noted that no attempt is made in this study to correlate the ISMR of Himalayan region with the agronomic productivity of this region. Since the primary focus of this study is to identify trends in the ISMR over IHR, no physio-dynamical aspects of change in ISMR has been investigated.

2 Data description

The rainfall datasets used in this study are daily gridded products from the Highly Resolved Observational Data Integration Towards the Evaluation of Water Resources (APHRODITE) project (Yatagai et al. 2009, 2012). These dataset was prepared by collecting observational data from thousands of stations across Asia, Himalaya, and mountainous areas in the Middle East. The APHRO_MA_V1101R2 data were used for this study. Qualities of the gridded rainfall products have always been under scrutiny due to their coarser horizontal resolution and APHRODITE products are no exception. Therefore, the quality of an earlier version of the APHRODITE data was evaluated by Rajeevan et al. (2008) for the period of 1980–2002 over India. Very high correlation coefficients were observed between APHRODITE and IMD data for the entire India excluding the regions of west coast and some parts of north eastern India. Their report has also mentioned that the basic deference between the IMD and APHORODITE data is the number of observation stations used. Andermann et al. (2011) has recently evaluated APHRODITE data with rain gauge and five other gridded rainfall products including TRMM rainfall data for the Nepal Himalaya and found that APHRODITE data provide a good temporal variability on a monthly to annual scale and even in some cases the daily variations. Andermann et al. (2011) has also concluded that the APHRODITE products can be used for better understanding of hydrological budget and discharge analysis of large basins than other gridded products. The APHRODITE

data has been increasingly used for rainfall and temperature analysis as has been done by Dimri et al. (2013) and Mathison et al. (2013).

The rainfall data were analyzed for the period 1951–2007 for the Indian summer monsoon months of June–September (JJAS). Along with the decadal trend of the JJAS rainfall of IHR, rainfall trends were also estimated for three normal periods as: NY1 representing the period 1951 to 1980, NY2 representing the period 1981 to 2007, and NY3 representing the period 1951 to 2007. The spatial resolution of the dataset was $0.25^\circ \times 0.25^\circ$. These daily gridded

rainfall data were categorized into three regular grid boxes over the region (i) 73.0–80.0 E and 31.0–36.0 N, (ii) 78.0–88.0 E and 26.0–31.0 N, and (iii) 88.0–97.5 E and 23.0–29.5 N to represent Western Himalayan region (WH), Central Himalayan region (CH), and Eastern Himalayan region (EH), respectively. Domains of these three IHRs are a partial modification of the same provided by Kulkarni et al. (2013). The topographical features of these selected regions are provided in Fig. 1. Although the principle focus of this study is to analyze the rainfall distribution for the Indian Himalayan region, considerable landmasses from

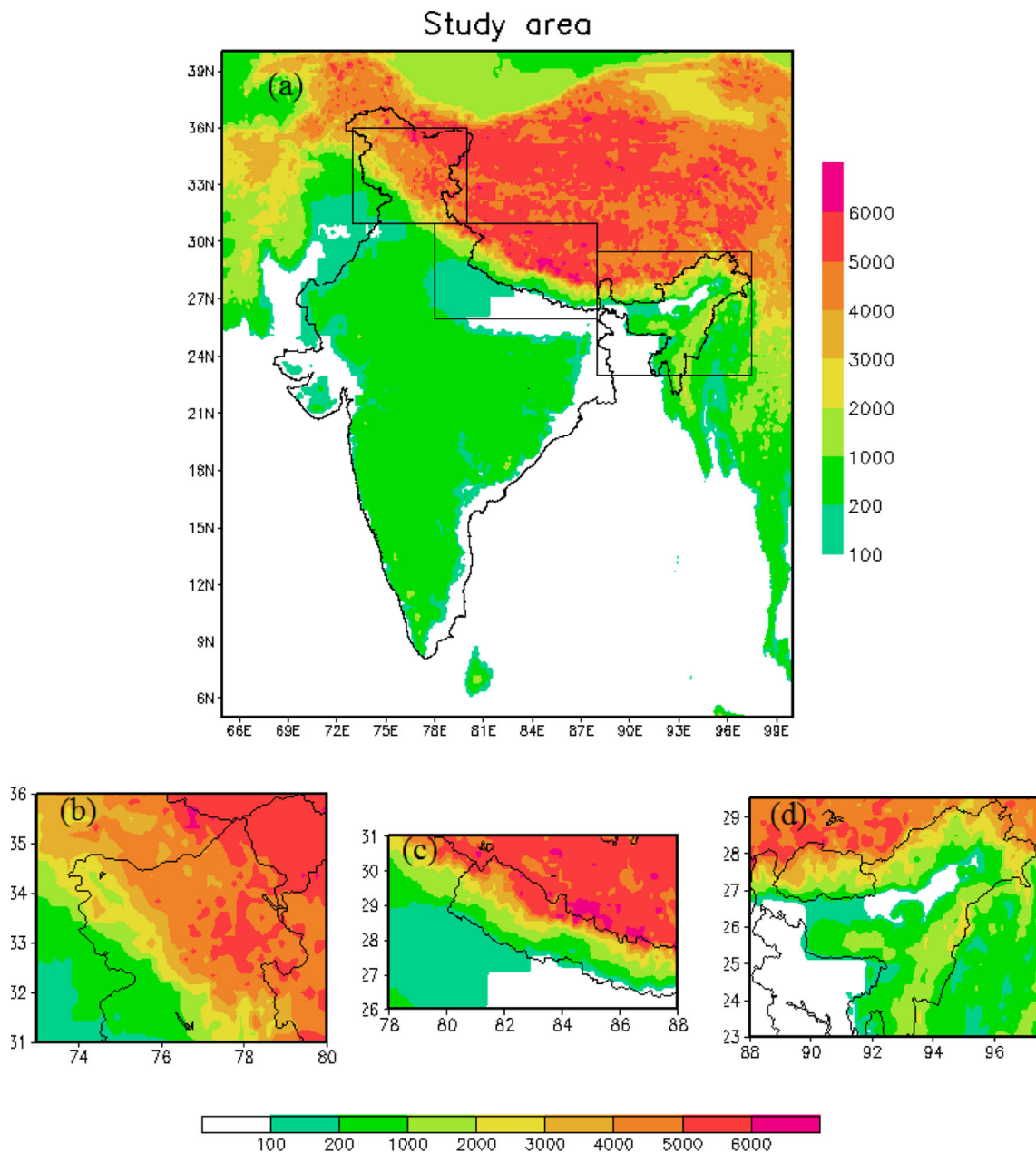


Fig. 1 a Represents the elevation of study area within the Indian region. Elevation (in meters) of the selected b western, c central, and d eastern Himalayan regions are shown in the bottom panel. Disclaimer: the geographical boundary used of is not necessarily be the political boundary

Nepal, Bangladesh, Myanmar, Pakistan, and Tibet are also included.

3 Methods

At first, spatial percentage departure of the decadal monsoon rainfall from the long-term JJAS mean rainfall of each region of IHR was estimated following Eq. 1:

$$PD_{Di} = ((\overline{R_{LT}} - \overline{R_{Di}})/\overline{R_{Di}}) * 100 \quad (1)$$

where PD_{Di} is the spatial percentage departure of the monsoon rainfall of i th year, $\overline{R_{LT}}$ is the average long-term mean JJAS rainfall computed over the period 1951–2007, and $\overline{R_{Di}}$ is the average JJAS rainfall of the i th decade. Next, the long-term trends and variabilities of JJAS rainfall of the IHR were estimated from the time series of daily gridded area average rainfall values of each region. Therefore, a single JJAS season had 122 points and the entire time series of 57 years consisted of 6954 values. Such average and maximum rainfall time series were produced for each region and are analyzed in Section 4.1. However, before trend analysis of the seasonal and average rainfall of IHR, changes in the frequency of occurrences of *strong* and *weak* phase were explored from the low-frequency intra-seasonal oscillation of the ISMR time series. For detail description of monsoon *active (strong)* and *break (weak)* phases, readers may look into Rajeevan et al. (2010) and Shukla (2013). However, here the low-frequency oscillations were produced following the procedure described in Mukherjee et al. (2011) where a 10–90 days bandpass Lanczos filter was used over the standardized anomaly of the average daily rainfall time series. The standardized anomaly of rainfall data was produced by removing the 57 year mean from the time series and by dividing the time series with its standard deviation. Observations of the filtered standardized anomaly > 1 were termed as *strong* periods and those < -1 were termed as *weak* periods (Fig. 2). The frequencies of these *strong* and

weak periods of each year were computed based on number of occurrences, and the linear trends were estimated. The results of this analysis are presented in Section 4.2.

Similarly, along with the estimation of trends in the seasonal (JJAS) average and maximum rainfall, trends were also estimated from the frequency of extreme rainfall events of each region (Fig. 3 upper panel) using Sen's slope estimator. The seasonal extreme rainfall events were defined as those events having rainfall > 80 mm/day for WH, > 100 mm/day for CH, and > 120 mm/day for EH. These limits were set by analyzing the percentile range and histograms of the daily rainfall of JJAS of each region (Fig. 3 bottom panel) and by partially modifying the extreme rainfall range provided by Goswami et al. (2006) for central India. The India Meteorological Department's classifications (Table 1 of Pattanaik and Rajeevan (2010)) of rainfall are also partially different from our ranges of extreme rainfall events. The Sen's slope estimator was then applied to each of these time series for decadal and long-term normals to identify trends. The empirical mode decomposition (EMD) method was only applied to the frequency index of extreme rainfall events to identify cycles of heavy rainfall occurrences. Brief descriptions of the Sen's slope estimator and EMD method are given below.

3.1 Sen's slope estimator

One of the most useful parametric models to detect trend is the Simple Linear Regression model. However, the method of linear regression requires the assumptions of normality of residuals. Many atmospheric variables including precipitation exhibit a marked skewness partly due to the influence of natural phenomena, and hence do not follow a normal distribution. Hence, in the present study, the Sen's slope estimator, which is a non-parametric method, has been used for the determination of the trend. The magnitude of trend is predicted by Sen's slope estimator which is a simple non-parametric estimator of trend and particularly useful

Fig. 2 Parts of the filtered standardized rainfall anomaly (mm/day) time series is represented where few strong or active (values > 1) and weak or break phases (values < -1) are indicated with arrows

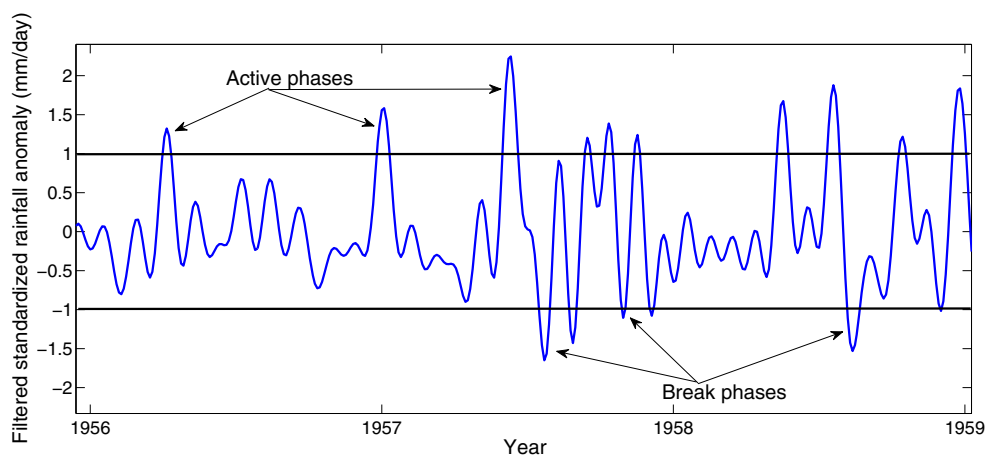
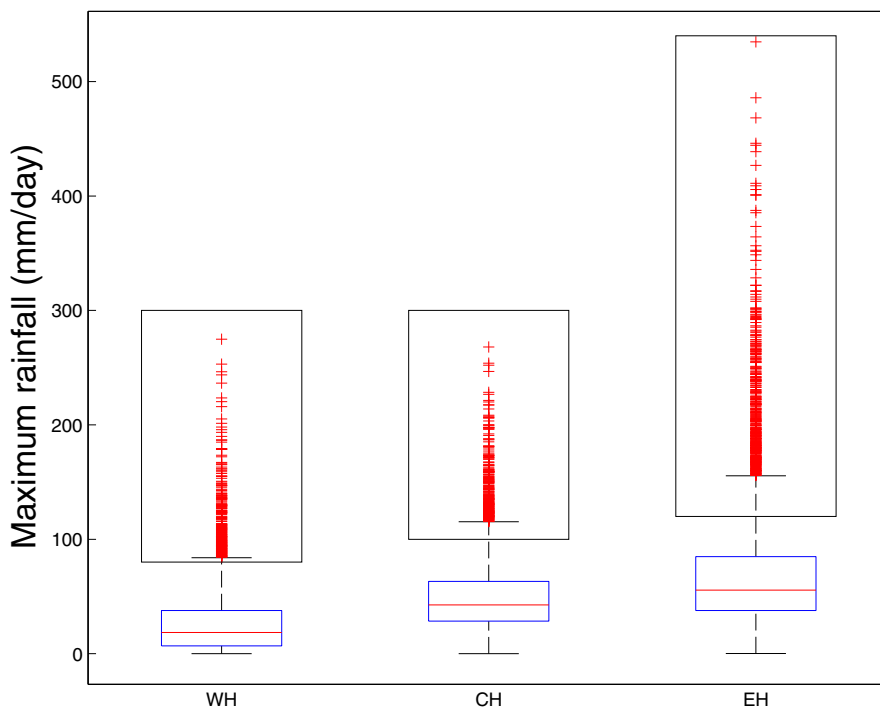
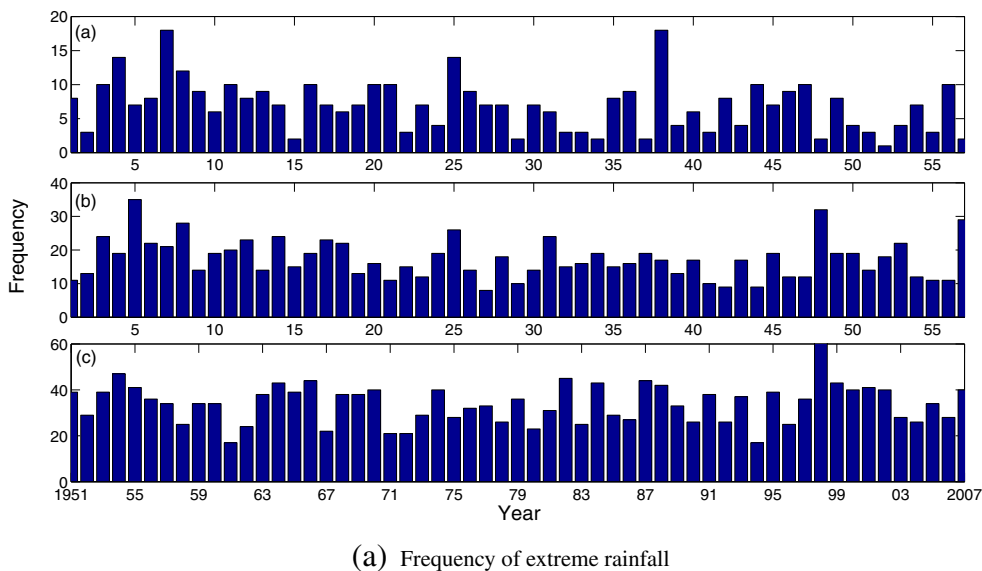


Fig. 3 Upper panel represents the frequency of extreme rainfall events for **a** western Himalaya (WH), **b** central Himalaya (CH), and **c** eastern Himalayan (EH) region. The *bottom figure* represents boxplots of the same. *Rectangles* are showing ranges of extreme rainfall values used for classification



for environmental monitoring (Sen 1968). This method offers many advantages that have made it useful in analyzing atmospheric data and is considered as robust to outliers, missing data, and non detects. To compute Sen’s trend estimator, first the slope (T_i) for each data point is calculated as:

$$T_i = \frac{x_j - x_k}{j - k}, i = 1, \dots, N \tag{2}$$

Where x_j and x_k are the data values at time j and k ($j > k$), respectively. The median value of the N values of T_i is represented as Sen’s estimator of trend. To obtain the median value of T_i , denoted as Q , the N values of T_i are ranked from smallest to largest (i.e., $T_1 \leq T_2 \dots T_{n-1} \leq T_n$) and the median slope is computed as:

$$Q_i = \begin{cases} T_{\frac{N+1}{2}} & \text{if } N \text{ is odd} \\ \frac{1}{2}(T_{\frac{N}{2}} + T_{\frac{N+2}{2}}) & \text{if } N \text{ is even} \end{cases} \tag{3}$$

Table 1 Monthly means (\pm standard deviation) of rainfall (mm/day) for western, central, and eastern Himalayan regions and their decadal and long-term values

Period	Region											
	WH				CH				EH			
	June	July	August	September	June	July	August	September	June	July	August	September
1951–1960	1 (0.52)	3.6 (1.64)	3.3 (1.12)	2 (–)	3.7 (2.13)	7.9 (1.65)	7.3 (1.10)	4.5 (1.71)	10.7 (0.82)	11.4 (1.65)	9.2 (0.56)	7.1 (1.90)
1961–1970	1 (0.57)	2.9 (0.52)	2.9 (0.44)	1.6 (–)	3.6 (1.10)	7.4 (0.67)	7.8 (0.75)	4.3 (1.53)	11.1 (1.85)	10.6 (0.82)	9.3 (1.04)	6.2 (0.65)
1971–1980	1.4 (0.55)	3.3 (0.98)	3.3 (1.27)	1.4 (0.63)	4.2 (1.54)	7.7 (0.90)	6.9 (0.67)	4.2 (1.37)	9.8 (1.87)	10.6 (0.94)	8.5 (1.09)	6.4 (1.40)
1981–1990	0.9 (0.53)	3.1 (0.95)	2.9 (0.46)	1.3 (–)	3.4 (1.21)	8.3 (0.84)	6.6 (0.99)	4.9 (1.57)	9.5 (1.08)	11.5 (1.96)	8.7 (1.44)	7.8 (1.06)
1991–2000	1.4 (0.81)	3.1 (1.30)	3.3 (2.18)	1.7 (–)	4.0 (1.54)	6.9 (0.96)	7.8 (0.59)	4.2 (0.66)	9.7 (0.86)	10.5 (1.61)	9.5 (0.78)	7.4 (1.17)
2001–2007	1.4 (0.78)	2.6 (1.15)	2.6 (0.56)	1.3 (0.75)	3.7 (0.78)	7.5 (1.00)	6.3 (1.01)	4.4 (0.85)	8.9 (1.27)	10.4 (1.77)	7.1 (1.25)	6.2 (2.09)
1951–1980	1.1 (0.59)	3.3 (1.20)	3.1 (1.09)	1.7 (–)	3.8 (1.69)	7.7 (1.20)	7.3 (0.99)	4.3 (1.60)	10.5 (1.54)	10.9 (1.18)	9 (1.00)	6.5 (1.61)
1980–2007	1.2 (0.75)	3 (1.12)	3 (1.37)	1.5 (–)	3.7 (1.26)	7.6 (1.11)	7.0 (0.85)	4.5 (1.17)	9.4 (1.05)	10.9 (1.79)	8.6 (1.19)	7.2 (1.38)
1951–2007	1.2 (0.67)	3.1 (1.15)	3.1 (1.22)	1.6 (–)	3.8 (1.49)	7.6 (1.17)	7.1 (0.95)	4.4 (1.42)	10 (1.37)	10.9 (1.49)	8.8 (1.09)	6.9 (1.52)

To test the null hypothesis of zero slope (i.e., no trend), Q_{med} is computed by a two-sided test at $100(1-\alpha)$ % confidence interval for true slope is computed by the non-parametric test based on the normal distribution. To compute the confidence limit, an estimate of the variance is required. Positive value of Q_i indicates an upward or increasing trend and a negative value of Q_i gives a downward or decreasing trend in the time series. The method is valid for n as small as 10 unless there are many ties.

3.2 Empirical mode decomposition

Traditionally, the Fourier spectral analysis method has been applied over time series of a phenomenon to infer different time scales embedded within the observation. However, applications of Fourier spectral analysis over nonlinear and non-stationary processes are known to produced frequencies with no physical significance (Huang et al. 1998). The Empirical Mode Decomposition (EMD) technique developed by Huang et al. (1998) provides an alternative method of decomposing a nonlinear and non-stationary time series into Intrinsic Mode Functions (IMFs), where each of these IMFs is unique, adaptive, and orthogonal to each other. Since the proposition of this method, EMD method has been extensively used in different studies such as Lundquist (2003) for temperature data, Duffy (2004) and Pan et al. (2002) for climatological data, Dwivedi and Mittal (2007) for monsoon rainfall data, Holder et al. (2011) for turbulence data, and so on. Such a diverse application of EMD method has been found to produce higher number of physically meaningful signals from the raw data than the traditional techniques.

For a signal $x(t)$, the EMD algorithm works following (Huang et al. 1998): (i) the identification of all extrema of $x(t)$, then (ii) forming a generic spline fitted envelope around $x(t)$ by interpolating between all maxima ($emax(t)$) and all minima ($emin(t)$), then (iii) computing the mean as: $m(t) = (emin(t) + emax(t))/2$, (iv) subtracting the envelope mean from the signal to yield the first component, $d(t)$, sometimes also called the detail, as $d(t) = x(t) - m(t)$, and (v) iterating steps (i)–(iv) with the detail $d(t)$ replacing $x(t)$ until the resulting $d(t)$ can be considered as zero-mean according to some stopping criterion. This procedure will produce finite number of IMFs of which few would be statistically significant.

In order to identify the cycles of extreme rainfall events over the IHR, the EMD technique was applied to the standardized anomaly of each frequency index of extreme rainfall events of WH, CH, and EH. The EMD method had produced several IMFs from a single frequency index of extreme events. The peak-to-peak distance of a single IMF would, therefore, provide the inter-annual cycles of occurrences of extreme events. However, not necessarily all the IMFs would be physically meaningful. Hence, to distinguish between the IMFs that were spurious (white noise) from those that carry physically significant information, the statistical test given by Wu and Huang (2003) was carried out. To avoid unnecessary description of the Wu and Huang (2003) test, we are briefly mentioning that this method estimates energy of each IMF and accepts only those signals whose energy fall within a predefined statistically significant acceptance level. In this analysis, only those IMFs were chosen which were physically meaningful within a 99 % acceptance level.

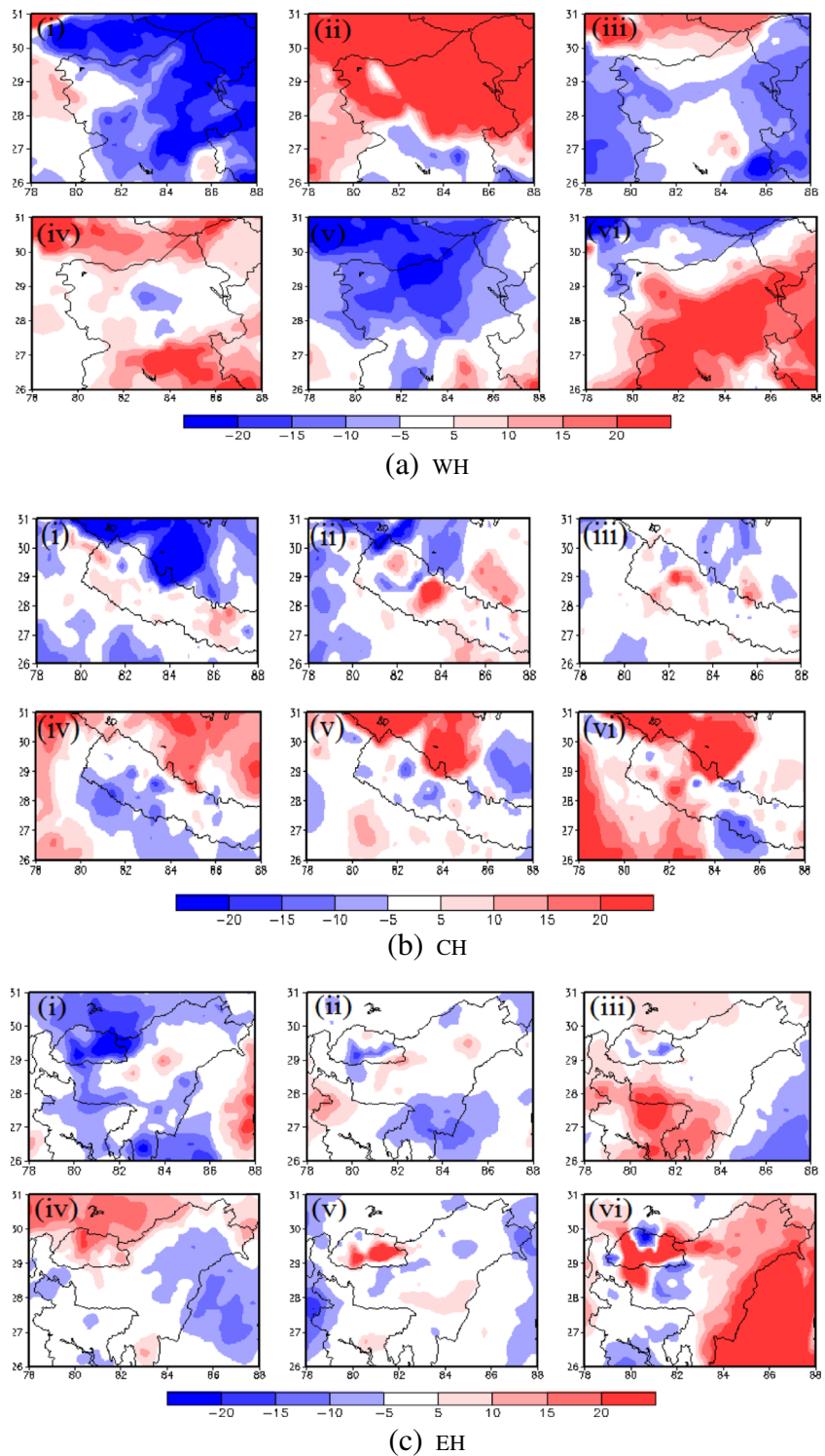
4 Results and discussion

4.1 Long-term rainfall variability in the IHR

Spatial distributions of the percentage departure (PD) values of decadal rainfall of each region are represented in Fig. 4.

It is eminent from Fig. 4a that the prescribed area of the WH region has clear decadal oscillating trend of receiving negative and positive rainfall departures from the long-term mean. However, this trend is spatially variable and such a decadal oscillating trend is not observed for the CH and EH regions (Figs. 4b, c). Rather for the CH, the upper

Fig. 4 Percentage departure of the decadal JJAS rainfall from the long-term average (1951–2007) is represented for **a** WH, **b** CH, and **c** EH. The notations (i) to (vi) indicate six decadal periods as: 1951–1960, 1961–1970, 1971–1980, 1981–1990, 1991–2000, and 2001–2007, respectively



Nepal Himalaya was consistently receiving lesser rainfall ($PD \leq -20\%$) for the periods 1951–1980 which changed to positive values during 1981–2007. This shows a significant change in the rainfall pattern in this region. On a decadal basis, most of the terai and middle Himalayan region of CH was found to receive normal rainfall ($-5\% \leq PD \leq 5\%$). For the EH region particularly over Bhutan, significant rain deficiency ($PD \leq -20\%$) was observed during 1951–60 period. Since 1981 onward, the area is getting positive departure.

The mean monthly rainfall distribution of the IHR is represented in Fig. 5 for the period 1951–2007. The long-term (1951–2007) averages (\pm std. dev.) of total rainfall of WH, CH, and EH for the 122 days of JJAS were found to be 274.2 (\pm 56.6), 704.1 (\pm 83.9), and 1115.8 (\pm 110.6) mm, respectively. The average of total rainfall over the EH region of our analysis was found to be 10.6 % higher than the values of 997.6 mm of Subash et al. (2011). However, it is to be noted that the results of Subash et al. (2011) were obtained only for the meteorological subdivisions of central and North-Eastern, India. The decadal mean and standard deviation of JJAS rainfall including NY1, NY2, and NY3 periods are provided in Table 1. When the average seasonal rainfall of CH region is compared with individually observed average station rainfall of Almora (624.8 mm) and Nainital (1701.6 mm) of Uttarakhand state (Joshi et al. 2013), the average seasonal rainfall obtained from this analysis was found to compare well with the station data of Almora (within 11.3 % deviation). Orientation of nearby mountain ridges and the location of this particular measurement station at Nainital have caused such a significant difference between these two values. With respect to the mean all India JJAS rainfall (852.4 ± 84.7 mm) estimated

by Parthasarathy et al. (1994), the EH was found to receive 30.9 % of excess rainfall on average, whereas the WH and CH were found to receive 210.7 and 17.4 % less rainfall. However, as explained earlier, our regional rainfall estimates were constrained by the inclusion of partial rainfall distributions over Pakistan, Bangladesh, Myanmar, Tibet, and Bhutan. Furthermore, averages (\pm std. dev.) of the total rainfall for the months of June to September of individual Himalayan region were compared with the all India values from Guhathakurta and Rajeevan (2008), and results are provided in Table 2. It is eminent from Table 2 that except for the EH region, the JJAS monthly averages of CH and WH are lower (ranges between 13.1–30.7 % for CH and 62.7–78.6 % for WH) than the all India values. However, the minimum deviation was observed for the month of August (13.1 and 62.7 %, respectively, for CH and WH), where as maximum deviations were observed for June (30.7 and 78.6 %, respectively, for CH and WH).

4.2 Changes in the frequency of strong and weak phases of ISMR

Figure 6 represents the changes in frequency of the *strong* and *weak* phases of monsoon intra-seasonal oscillations over the IHR. It is eminent from Fig. 6a, c, and e that the entire Himalayan region is experiencing shortage of *strong* monsoon periods on a long-term basis, i.e., for the period NY3: 1951–2007. The overall decreasing trend (slopes of linear regression) in the frequency of *strong* phases for WH, CH, and EH were found to be -0.07 , -0.11 , and -0.05 , respectively. The decreasing trend for the WH and CH was found to be statistically significant within a p value ≤ 0.10 . Clearly, the central Himalaya is the most affected region

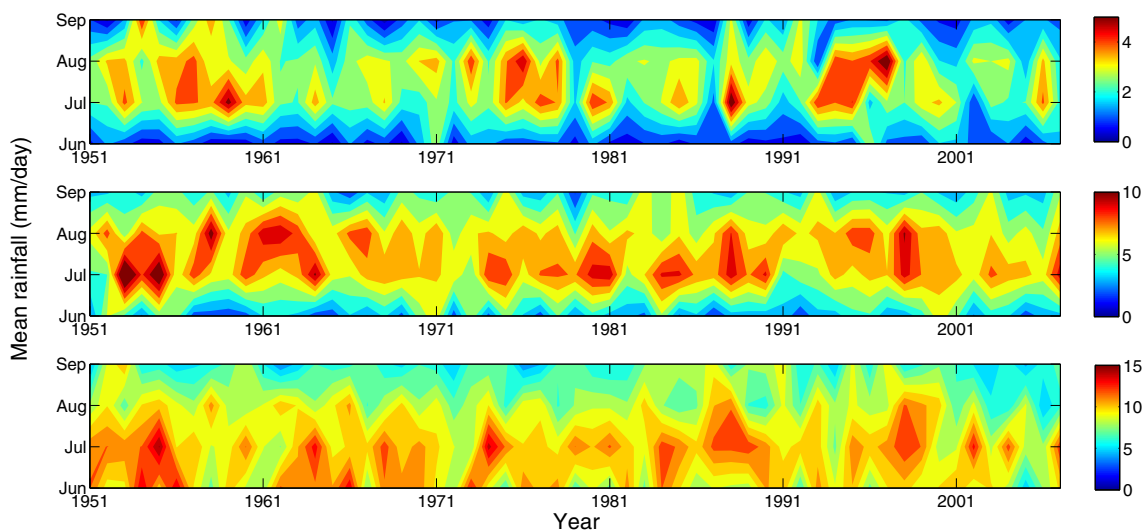


Fig. 5 The mean monthly variation (JJAS) of average rainfall (mm/day) for the period of 1951–2007 is represented for (*upper panel*) WH, (*middle panel*) CH, and (*bottom panel*) EH

Table 2 Comparison of average (\pm standard deviation) monthly rainfall for the monsoon period for western, central, and eastern Himalaya (WH, CH, and EH) with the all India (AI) averages obtained from Guhathakurta and Rajeevan (2008)

Region	June	July	August	September
WH	34.9 (\pm 15.3)	97.1 (\pm 29.0)	95.2 (\pm 26.7)	46.9 (\pm 26.6)
CH	113.1 (\pm 37.1)	236.7 (\pm 48.7)	221.7 (\pm 39.5)	132.5 (\pm 33.7)
EH	299.6 (\pm 56.0)	337 (\pm 52.2)	273 (\pm 49.4)	206.3 (\pm 45.4)
AI	163.4 (\pm 29.5)	286.7 (\pm 35.3)	255.3 (\pm 30.6)	171.8 (\pm 32.8)

where the frequency of *strong* phases of ISMR is sharply declining. When the frequency trend of strong phases was analyzed for NY1 and NY2 periods, all negative slopes (-0.23 , -0.29 , and -0.13) were observed for NY1 over WH, CH, and EH. However, positive slopes (0.06 and 0.12) were observed in the frequency of strong phases, respectively, for WH and EH, for NY2 period. This signifies that although the overall frequency trend of strong phases of monsoon is decreasing since 1951, enhanced number of strong phases was observed in the recent past for most of the IHR.

Surprisingly, the overall frequency of monsoon weak phases was also found to be decreasing for the period of 1951 to 2007 for the entire IHR (Fig. 6b, d, f). The decreasing trends of CH and EH were found to be statistically significant within p value ≤ 0.05 . Trends in the frequency of monsoon weak phases over the period of 1951–2007 were found to be -0.04 , -0.06 , and -0.08 , respectively, for WH, CH, and EH. Trends in the weak phases of rainfall for the normal period of NY1 were found to be -0.17 , -0.19 , and -0.12 for WH, CH, and EH. The same were found to be 0.03 , -0.01 , and -0.07 for the normal period NY2. These results signify that in the recent past, WH region of the IHR is experiencing enhanced number of strong and weak phases of ISMR, whereas CH and EH are experiencing decreased number of weak phases. Figure 4(b i–vi) depicts the decadal spatial percentage departure of rainfall

from long-term mean for the CH. However, when the area averaged rainfall for each season is analyzed for strong and weak phases of CH, negative trend was observed for the entire NY3 period. Now, if we look into Table 3 for average rainfall trend, we find that a significant enhancement in the average seasonal rainfall trend during 1981–2000. This significant enhancement of average rainfall (particularly during 1991–2000) accounts for the changes in the PD values shown in Fig. 4(b i–vi) of CH.

4.3 Trends analysis of seasonal average, maximum rainfall and frequency of extreme rainfall events

Before analyzing the trends of ISMR, variabilities of the JJAS rainfall of each year were estimated with respect to the seasonal rainfall. Figure 7 represents the % of total seasonal rainfall of JJAS months. It is evident from Fig. 7 that the EH region experiences almost homogeneous rainfall distribution for the months of June to August (Fig. 7c), where occasionally maximum seasonal rainfall events ($> 30\%$ of seasonal rainfall) were occurring for the months of June and July. However, for the CH and WH regions, July and August were the 2 months which explained most of the variances of seasonal total rainfall. On average, individual months of June to September were found to represent 12.9, 35.3, 34.8, and 16.7 % of the total rainfall of the WH region; 15.9, 33.6, 31.6, and 18.7 % of the total rainfall of the CH region; and

Fig. 6 Changes in the frequency of strong (a, c, e) and weak (b, d, f) phases of the ISMR is represented for the Western Himalaya (a, b), central Himalaya (c, d), and eastern Himalaya (e, f). The red dashed lines represent trends. Only those p values are shown in the diagram which are ≤ 0.10

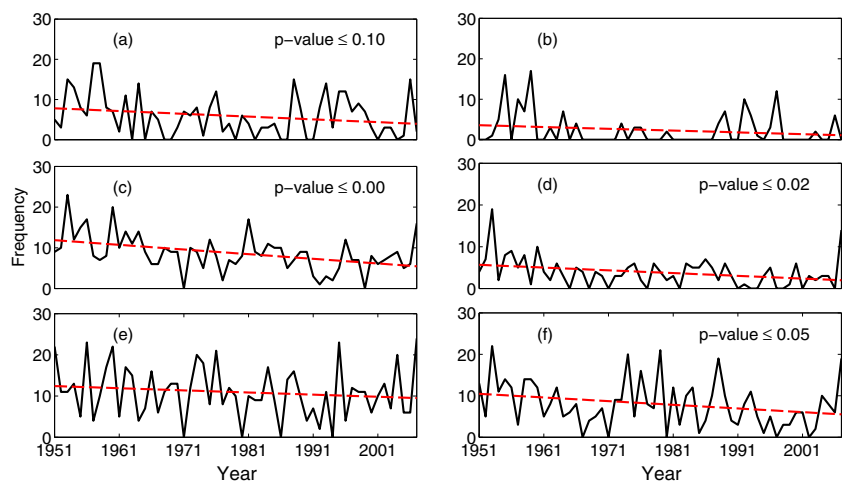


Table 3 Sen's estimator of slope (mm/day) for the seasonal average, maximum, and extreme rainfall events

Period	Average rainfall trend			Maximum rainfall trend			Extreme rainfall trend		
	Region			Region			Region		
	WH	CH	EH	WH	CH	EH	WH	CH	EH
1951–1960	0.10	0.03	−0.09	1.32	0.25	−1.31	0.33	0.00	0.00
1961–1970	−0.04	−0.06	0.10	−0.49	−0.28	2.11	−0.14	−0.20	0.88
1971–1980	0.01	0.00	−0.02	−0.36	0.32	0.24	−0.14	−0.33	0.44
1981–1990	0.04	0.01	0.08	0.62	−0.29	−0.84	0.38	−0.80	−0.83
1991–2000	0.02	0.18	0.06	0.22	1.07	1.89	0.00	1.00	0.75
2001–2007	0.02	−0.10	−0.22	0.60	−0.12	−0.25	0.50	−0.50	0.80
1951–1980	0.00	−0.01	−0.04	−0.05	−0.13	−0.43	−0.08	−0.20	−0.29
1980–2007	0.00	−0.01	−0.05	−0.08	−0.02	−0.06	0.00	0.00	0.10
1951–2007	0.00	0.00	−0.01	−0.12	0.00	−0.01	−0.08	−0.04	0.00

The italic values are statistically significant at a p value ≤ 0.05

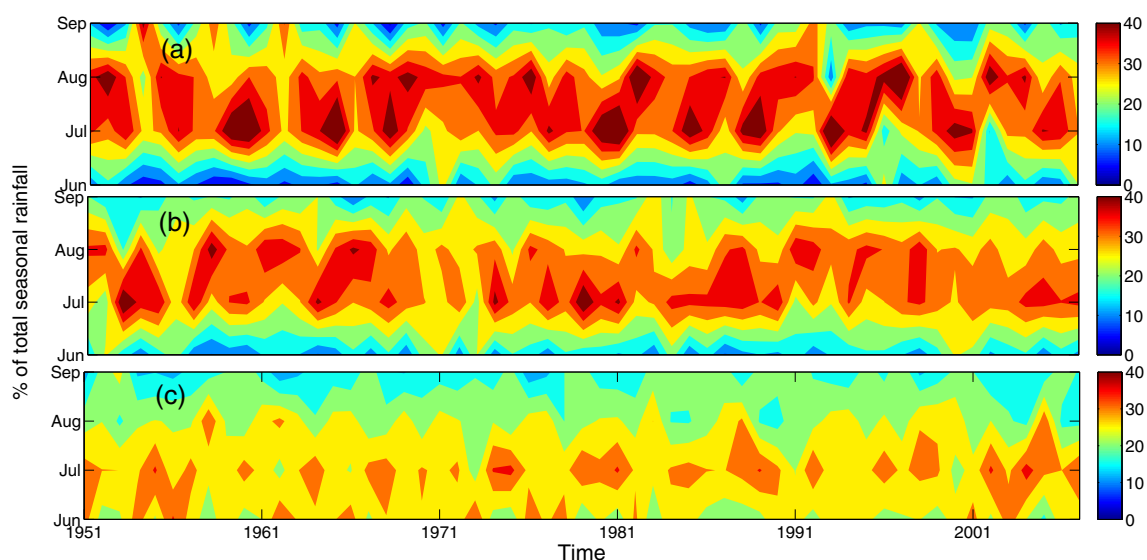
26.8, 30.2, 24.4, and 18.4 % of the total rainfall of the EH region, respectively.

In order to further explore the % changes in the monthly total rainfall values to the seasonal total rainfall, year-wise trends (slopes of linear regression) were produced for each Himalayan region and for each month (Fig. 8). Over the WH and CH regions, an increasing trend in the % contribution of total seasonal rainfall by the month of June was observed (slope = 0.11 and 0.02 of Fig. 8a, e), whereas the trends were found to decrease for August and September.

However, for the EH, increasing trends in the % contribution of total seasonal rainfall were observed for July and September (slope = 0.03 and 0.05 of Fig. 8j, l), whereas the month of June and August were having negative trend (Fig. 8i, k).

The seasonal average, maximum, and extreme rainfall trends of the IHR were estimated using a nonparametric statistical test, Sen's slope estimator. Along with the three normal periods (NY1, NY2, and NY3), seasonal rainfall trends were also estimated for individual decade and results are represented in Table 3. It is eminent from Table 3 that no statistically significant decade to decade rainfall trend was observed for the entire IHR when seasonal average, maximum, and extreme rainfalls are considered except for the positive rainfall trend of 0.18 mm/day during 1991–2000. However, decade-to-decade variation in the rainfall slopes values was observed for all three classes of rainfall events.

When the trends of three classes of rainfall events (average, maximum rainfall, and frequency of extreme rainfall)

**Fig. 7** Percentage contribution of individual JJAS months to the total seasonal rainfall is represented for the **a** WH, **b** CH, and **c** EH region

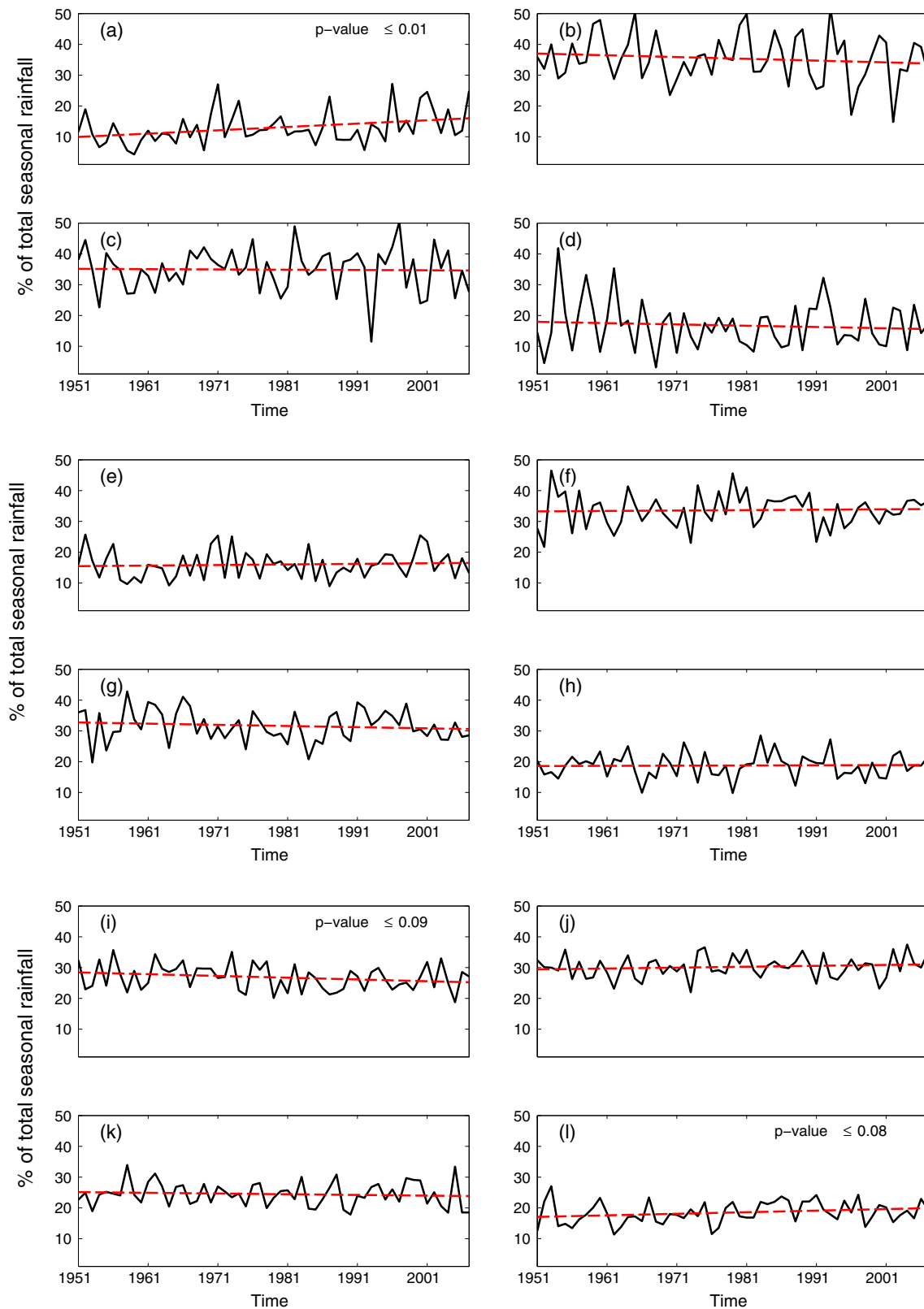


Fig. 8 Trends in the % contribution of individual JJAS months to the total seasonal rainfall are represented for the **a–d** WH, **e–h** CH, and **i–l** EH regions. Trends in the % contribution of total seasonal rainfall for June are represented in subplots (**a**, **e** and **i**); the same for July are represented in subplots (**b**, **f**, and **j**); for August are represented in

subplots (**c**, **g**, and **k**); and for September are represented in subplots (**d**, **h**, and **l**). The *red dashed lines* are produced from a linear regression representing trends. Only those *p* values are shown in the diagram which are ≤ 0.10

Table 4 Statistically significant (within a confidence interval of 95 %) IMFs of seasonal extreme rainfall frequencies for three Himalayan regions

Region	WH			CH		EH	
	1	3	4	1	3	1	2
IMF No.							
Mean time (\pm standard deviation)	2.7 (0.99)	12.2 (4.5)	40.0 (–)	2.94 (0.89)	15.3 (3.21)	2.7 (0.87)	5.8 (1.57)
Fev	0.53	0.15	0.08	0.53	0.11	0.61	0.22

T and *FEV* represent the temporal frequency (yearly) and fraction of explained variances of each IMF

were considered for the WH sector for three normal periods (NY1, NY2, and NY3), the maximum rainfall events were found to be decreasing for all three normal periods (-0.05 , -0.08 , and -0.12), of which trend for the NY3 period (-0.12) was found to be statistically significant (p value < 0.05). The extreme rainfall events were also found to be decreasing for the WH region for the normal period NY1 and NY3, of which trend for the NY3 period was found to be statistically significant (p value < 0.05). The average monsoon rainfall trend analysis of Bhutiyani et al. (2010) for the northwestern Himalaya, however, represents a statistically significant negative trend which was absent in our analysis.

All the three classes of rainfall events (average, maximum rainfall, and frequency of extreme rainfall) were found to be decreasing for the CH region for NY1 and NY2 periods except for zero trend of frequency of extreme rainfall events of CH region. However, only the frequency of extreme rainfall events trend of CH for NY1 period (-0.20) was found to be statistically significant within a p value < 0.05 . The trend analysis of extreme rainfall event frequencies by Joshi et al. (2013) using two station data of CH region (Almora and Nainital) has also revealed a negative trend for the monsoon period. However, similar to the results of Borgaonkar et al. (1998), trends reported in Joshi et al. (2013) were not statistically significant within a p value < 0.05 . The NY2 period of EH region was found to be the only period when number of frequency of extreme rainfall events was increasing; however, the slope value (0.10) was not statistically significant within a p value < 0.05 .

4.4 Yearly cycles of extreme events from EMD analysis

Results of EMD analysis are presented in Table 4. After the statistical test of Wu and Huang (2003), it was observed that IMF numbers 1, 3, and 4 of WH; 1 and 3 of CH; and 1 and 2 of EH were physically significant (within 99 % acceptance level). The fraction of explained variances ($Fev =$ ratio of variance of each IMF to the variance of the total data) of these selected IMFs was found to be the highest. Finally,

when the cycles of occurrences of extreme events were estimated from the IMFs, a dominant cycle of ~ 2.7 years was observed for all three regions. Similar monsoonal rainfall cycles varying between 2.2 to 2.9 years were also observed by Bhutiyani et al. (2010) for the north-western Himalayan region, but not for the extreme events. This might suggest the occurrences of extreme rainfall events are highly associated with the cycles of monsoon rainfall. The WH, CH, and EH were also found to have cycles of 12.2, 15.3, and 5.8 years, respectively. Statistically, these signals are significant with a range of 99 %.

5 Conclusion

Although several studies of the recent past have reported the trends of seasonal and extreme rainfall events over India for a wide range of spatial and temporal scale, analyses of rainfall trend for the entire IHR are rare. The constrained nature of the rainfall distribution originating due to local complex topography is the main reason behind the ambiguities observed during analyses of rainfall trends of the IHR. This study presents trend analyses of ISMR over the IHR from a wider perspective by incorporating the large mountainous region of Himalaya in three segments. Some of the important findings of this study indicate that the entire Himalayan region is experiencing shortages of monsoon *strong* phase as trend of monsoon *strong* phase frequency is declining. Surprisingly, the trend in the monsoon *weak* phase frequencies is also found to be declining. The % contribution to the total seasonal rainfall by the month of June rainfall is found to be increasing for the central and western Himalaya, whereas the same for July and September is found to be increasing for Eastern Himalaya. Trends in the extreme rainfall events over IHR are found to be mostly negative over the period 1951–2007; however, no discernible trend is observed for the recent past (1980–2007). A common cycle of 2.7 years of extreme rainfall event frequencies is also observed for the entire Himalayan region. Since our particular objective of this study was to find trends in several monsoon rainfall indices, physio-dynamical aspects of these changing trends

are not investigated. However, investigation on the variation in the moist static energy and convective instabilities of the mountain region is assumed to provide necessary justification of this changing rainfall trends.

Acknowledgment Authors are thankful to the APHRODITE's Water Resources project, supported by Environment Research and Technology Development Fund of the Ministry of the Environment, Japan, for the rainfall data. This work is a part of an In-House project of Watershed Process Management Group of GBPIHED, Kosi-Katarmal, Almora, India.

References

- Andermann C, Bonnet S, Gloaguen R (2011) Evaluation of precipitation data sets along the himalayan front. *Geochem Geophys Geosyst* 12:Q07,023–Q07,039
- Archer D, Fowler H (2004) Spatial and temporal variations in precipitation in the Upper Indus Basin, global teleconnections and hydrological implications. *Hydrol Earth Syst Sci* 8:47–61
- Barros A, Kim G, Williams E, Nesbitt S (2004) Probing orographic controls in the Himalayas during the monsoon using satellite imagery. *Nat Hazards Earth Syst Sci* 4:29–51
- Barry R (2008) Mountain weather and climate. Cambridge University Press, Cambridge
- Bhutiyan M, Kale V, Powar N (2010) Climate change and the precipitation variations in the Northwestern Himalaya: 1866006. *Int J Climatol* 30:535–548
- Borgaonkar H, Pant G, Kumar K (1998) A study of seasonal pattern and magnitudes of climatological inputs to the hydrology of Western Himalaya. In: Tappeiner U, Ruffini FV, Fumai M (eds) *Head-Water'98 hydrology, water resources and ecology of mountain areas*
- Dimri A, Yasunari T, Wiltshire A, Kumar P, Mathison C, Ridley J, Jacob D (2013) Application of regional climate models to the Indian winter monsoon over the western Himalayas. *Sci Total Environ* 468–469S:S36–S47
- Duffy D (2004) The application of Hilbert-Huang transforms to meteorological datasets. *J Atmos Ocean Technol* 21:599–611
- Dwivedi S, Mittal A (2007) Forecasting the duration of active and break spells in intrinsic mode functions of indian monsoon intraseasonal oscillations. *Geophys Res Lett* 34(L16827):1–5. doi:10.1029/2007GL030540
- Fowler HJ, Archer DR (2006) Conflicting signals of climatic change in the upper indus basin. *J Clim* 19(17):4276–4293
- Gadgil S, Rao P (2000) Famine strategies for a variable climate—a challenge. *Curr Sci* 78:1203–1215
- Goswami B, Venugopal V, Sengupta D, Madhusoodanan M, Xavier P (2006) Increasing trend of extreme rain events over India in a warming environment. *Science* 314:1442–1445
- Guhathakurta P, Rajeevan M (2008) Trends in the rainfall pattern over India. *Int J Clim* 28:1453–1469
- Holder H, Bolch A, Avissar R (2011) Processing turbulence data collected on board the helicopter observation platform (HOP) with the empirical mode decomposition (EMD) method. *J Atmos Ocean Technol* 28:671–683. doi:10.1175/2011JTECHA1410.1
- Huang N, Shen Z, Long S, Wu M, Shih H, Zheng Q, Yen N, Tung C, Liu H (1998) The empirical mode decomposition and the hilbert spectrum for nonlinear and non-stationary time series analysis. *Proc R Soc Lond Ser A* 454:903–995
- IPCC (2007) *Ipcc fourth assessment report*. Tech. rep., Inter governmental pannel on climate change
- Jones P, Moberg A (2003) Hemispheric and large-scale surface air temperature variations: an extensive revision and an update to 2001. *J Clim* 16:206–223
- Joshi S, Kumar K, Joshi V, Pande B (2013) Rainfall variability and indices of extreme rainfall-analysis and perception study fortwo stations over central himalaya. *Nat Hazards* doi:10.1007/s11069-013-1012-4
- Khan A (2001) Analysis of hydro-meteorological time series: searching evidence for climate change in the Upper Indus basin. Tech. rep., International Water Management Institute (IWMI), Pakistan, Lahore Working Paper 23
- Kulkarni A, Patwardhan S, Krishna Kumar S, Karamuri A, Krishnan R (2013) Projected climate change in the Hindu Kush-Himalayan region by using the high-resolution regional climate model PRECIS. *Mt Res Dev* 33:142–151
- Kumar V, Jain S (2010) Trends in seasonal and annual rainfall and rainy days in Kashmir Valley in the last century. *Quat Int* 212:64–69
- Kumar V, Singh P, Jain S (2005) Rainfall trends over Himachal Pradesh, Western Himalaya, India In: *Proceeding conference development of hydro power projects—a prospective challenge*. Shimla
- Lundquist J (2003) Intermittent and elliptical inertial oscillations in the atmospheric boundary layer. *J Atmos Sci* 60:2661–2673
- Mathison C, Wiltshire A, Dimri A, Falloon P, Jacob D, Kumar P, Moors E, Ridley J, Siderius C, Stoffel M, Yasunari T (2013) Regional projections of North Indian climate for adaptation studies. *Sci Total Environ* 468–469S:S4–S17
- Mukherjee S, Shukla R, Mittal A, Pandey A (2011) Mathematical analysis of a chaotic model in relevance to monsoon ISO. *Meteorol Atmos Phys* 114:83–93. doi:10.1007/s00703-011-0159-3
- Pan J, Yan X, Zheng Q, Liu W, Klemas V (2002) Interpretation of scatterometer ocean surface wind vector EOFs over the northwestern Pacific. *Remote Sens Environ* 84:53–68
- Pant G, Borgaonkar H (1984) Climate of the hill regions of Uttar Pradesh. *Himal Res Dev* 3:13–20
- Pant G, Rupa Kumar K, Borgaonkar H (1999) Climate and its long-term variability over the Western Himalaya during the past two Centuries. In: Dash SK, Bahadur J (eds) *The himalayan environment*. New Age International (P) Limited Publishers, New Delhi
- Parthasarathy B, Munot A, Kothawale D (1994) All-India monthly and seasonal rainfall series: 1871-19930. *Theor Appl Clim* 49:217–224
- Pattanaik D, Rajeevan M (2010) Variability of extreme rainfall events over India during southwest monsoon season. *Meteorol Appl* 17:88–104
- Rajeevan M, Bhate J, KD K, Lal B (2006) High resolution daily gridded rainfall data for the Indian region: Analysis of break and active monsoon spells. *Current Sci* 91:296–306
- Rajeevan M, Bhate J, Jaswal A (2008) Analysis of variability and trends of extreme rainfall events over India using 104 years of gridded daily rainfall data. *Geophys Res Lett* L18707:1–6
- Rajeevan M, Gadgil S, Bhate J (2010) Active and break spells of the Indian summer monsoon. *J Earth Syst Sci* 119(3):229–247
- Sen P (1968) Estimates of the regression coefficient based on Kendall's tau. *J Am Stat Assoc* 39:1379–1389
- Sharma K, Moore B, Vorosmarty C (2000) Anthropogenic, climatic and hydrologic trends in the Kosi Basin, Himalaya. *Clim Chang* 47:141–165
- Shrestha A, Wake C, Dibb J, Mayweski P (2000) Precipitation fluctuations in the Nepal Himalaya and its vicinity and relationship with some large scale climatological parameters. *Int J Climatol* 20:317–327

- Shukla R (2013) The dominant intraseasonal mode of intraseasonal South Asian summer monsoon. *J Geophys Res* 119:635–651
- Singh P, Kumar N (1997) Impact assessment of climate change on the hydrological response of a snow and glacier melt runoff dominated Himalayan river. *J Hydrol* 193:316–350
- Singh P, Kumar V, Thomas T, Arora M (2008) Changes in rainfall and relative humidity in different river basins in the northwest and central India. *Hydrol Process* 22:2982–2992
- Singh R, Sen-Roy S (2002) Climate variability and hydrological extremes in a Himalayan catchment. In: ERB and Northern European FRIEND Project 5 Conference. Slovakia
- Subash N, Sikka A, Ram Mohan H (2011) An investigation into observational characteristics of rainfall and temperature in central India - a historical perspective 1889-2008. *Theor Appl Climatol* 103:305–319
- Wu Z, Huang N (2003) A study of the characteristics of white noise using the empirical mode decomposition method. *Proc R Soc Lond Ser A* 460:1597–1611
- Yatagai A, Arakawa O, Kamiguchi K, Kawamoto H, Nodzu M, Hamada A (2009) A 44-year daily gridded precipitation dataset for Asia based on a dense network of rain gauges. *Sci Online Lett Atmos* 5:137–140
- Yatagai A, Kamiguchi K, Arakawa O, Hamada A, Yasutomi N, Kito H (2012) APHRODITE: Constructing a long-term daily gridded precipitation dataset for Asia based on a dense network of rain gauges. *Bull Amer Meteorol Soc* 93:1401–1415